2 *Heating unevenness – dependence on oven properties, food dielectric properties and geometries*

2.1 Introduction

Dielectric properties have already been defined and dealt with in Chapter X. Briefly, they are expressed by two quantities, the real (relative) permittivity ε' (sometimes called "dielectric constant" even if it varies) , and the loss factor ε'' (Risman, 1991). It is very convenient for many computations to bring these together to the complex permittivity $\varepsilon = \varepsilon' - j\varepsilon''$, where j is the complex unit $\sqrt{-1}$. ε'' may include a contribution by conductivity; see chapter 1, section 1.4.

Detailed studies of the dielectric properties of foods began in the 1960's, when industrial microwave heating and microwave ovens became increasingly common. It was generally thought that improved knowledge about these properties would quite immediately assist in improving the engineering designs of microwave ovens, as well as development of microwave snacks and meals in the food industry. But this did not happen. The main reason was a poor understanding in the food industry of the many kinds of interactions between microwave fields and dielectric bodies – the food loads. There was also a rather weak development of microwave oven characteristics – the so-called multimode concept dominated, particularly in the US.

To-day, most of the microwave-food interactions are understood, but literature descriptions are scarce and scattered. The separation into distinguishable phenomena which are discussed here has turned out to be very fruitful in the research and development in some industries. Several of the phenomena have been qualitatively and quantitatively dealt with before at only microwave conferences and symposia. A knowledge about them assists in development of ready meals and in the understanding of causes of problems that may then occur. With numerical modelling being increasingly used in industry, knowledge about the individual phenomena will also assist in developing improved goal functions for microwave food heating and processing. Those described in the literature are still, with only very few exceptions, for example by Sundberg (1998), based on approaches of overall heating evenness, without particular considerations of food item tolerances and microwave oven property variables.

Characterisation of microwave ovens is basically outside the scope of this chapter, but a knowledge of some properties is necessary in order to understand how the dielectric properties influence the heating results. Cavity *volume mode* basics is addressed in sections 2.3 and 2.4, and their influence on horizontal heating patterns in section 2.11.2. A more comprehensive treatment is given by Risman (2003), including a measurement method for determination of cavity volume mode characteristics. The strength of *underheating trapped modes* can be measured by heating experiments described in section 2.5. Only these two kinds of modes are geometrically bound by the cavity, making it possible to even out patchy heating patterns by load movement such as rotation.

Twelve load-dependent phenomena are also dealt with, some of which are partially interrelated. They are:

- The penetration depth (section 2.2)
- Internal vertical standing waves in large loads (section 2.6)
- Simultaneous heating of loads with different permittivities (section 2.7)
- Influences by different ε'', with the same ε' – and the ε'' increase runaway effect (section 2.8)
- The edge overheating effect (section 2.9)
- Heating of small isolated round objects (section 2.10.2)
- The exploding egg effect (section 2.10.3)
- The cold rim effect (section 2.10.4)
- Particular heating effects in uneven top surfaces (section 2.11.4)
- The hot corner effect (section 2.11.6)
- The burnt stripe runaway effect (section 2.11.7)
- The multiple load item proximity effect (section 2.11.8)

All these phenomena are bound to the load itself and are therefore not evened-out much by load movement. However, the strength of some of them also depends on the cavity mode characteristics. The very significant variability between microwave ovens thus remains a problem for the food industry.

2.2 The microwave penetration depth

Actually, the only important microwave interaction property directly related to the dielectric properties that began to play an early role in industry was the penetration depth (depth of power penetration), usually labelled d_p.

d_p is defined as the depth below the surface of a

1. large,

2. flat and
3. infinitely thick load item
4. irradiated from straight above by
5. a plane microwave,
6. at which $\frac{1}{e}$ (about 37 %) of the power density at the surface remains. Due to the exponential decay of the power density, this depth is also that below which $\frac{1}{e}$ of the total power is deposited.

There is a quite complicated formula given in most textbooks, but a much simpler and still exact expression for d_p is

$$d_p = -\lambda_0/(4\pi \cdot \mathrm{Im}\sqrt{\varepsilon}) \qquad [2.1]$$

where λ_0 is the free space wavelength of the microwaves and ε is the complex ε'–jε''. The expression can easily be evaluated with a calculator accepting complex numbers.

If $\varepsilon''/\varepsilon'$ is less than about 1, an approximate formula

$$d_p = \lambda_0 \cdot \sqrt{\varepsilon'}/(2\pi \cdot \varepsilon'') \qquad [2.2]$$

can be used. This indicates that d_p is less sensitive to deviations in ε' than to deviations in ε''.

Actually, the complete definition of d_p above indicates what may vary in real practical situations. When items 1 to 3 above are not fulfilled:

- additional phenomena may occur near the edges of a flat food surface (see section 2.9);
- additional phenomena may occur in thin loads (see section 2.6);
- it is unclear what happens inside rounded food items (see section 2.10).

All conditions 1 to 4 above may change the power deposition pattern, making the "d_p concept" less useful in many practical situations.

2.3 *Cavity modes*

2.3.1 *Geometric optics conditions*

Some volume mode concepts must now be introduced. A starting point is then the angle of incidence in geometric optics; see figure 2.1.

The relationship between the incident and transmitting angles is the well-known Snell's law (law of refraction):

$$\sin\theta^i = \sqrt{|\varepsilon|} \cdot \sin\theta^t \qquad [2.3]$$

The fact that the wave is no longer transmitted perpendicularly into the dielectric results in a shorter penetration depth as calculated straight inwards from the surface. One can show that $\sqrt{\varepsilon'}$ in equation 2.2 is replaced by $(|\varepsilon - \sin^2\theta^i|)^{½}$. The difference will become

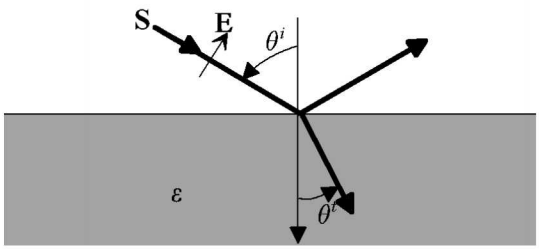

Figure 2.1. Incident (θ^i) and transmitting (θ^t)angles of a plane wave incient on a large dielectric. The electric (E) field is drawn for TM polarisation.

significant only with low ε' values. As an example for a typical compact frozen food item, ε=4–j1 gives d_p = 39,2 mm, which is reduced to 34,2 mm for striking incidence (θ^i = 90°).

Another characteristic is the wave polarisation. A TE-polarised incident wave has its electric (E) field parallel to the surface (and thus its magnetic (H) field at an angle to the surface). The opposite applies to TM-polarised waves.

2.3.2 *Waveguide and cavity modes*

It is found that microwave fields in closed metal tubes or cavities assume characteristic and discrete single or multiple (added) patterns. These can be of many kinds, examples being the single pattern in a coaxial line and the multiple interference pattern in large metal cavities. Theoretically, there is only one solution to the wave equation in each such case, but this solution can almost always be separated into dependent, partially dependent or independent simpler *modes, which are each of the possible configurations of the fields in a given domain in space.*

In microwave heating applications, separation of the overall field pattern into modes is a very important tool for both understanding of mechanisms and for system synthesis. The understanding of volume mode interaction with large loads is greatly simplified by a partial analogy to plane wave (geometric optics) radiation. The use of image sets of plane waves to represent waveguide modes is generally called the *electromagnetic ray concept.*

Figure 2.2 shows two TM-polarised waves with the same ($\pm\theta^i$) incidence angles towards a dielectric at the bottom of a two-dimensional waveguide. The vertical (z-directed) wavelength λ_g is an important parameter and the figure can be used to deduce the following important relationship:

$$\lambda_g = \lambda_0/\cos\theta^i \qquad [2.4]$$

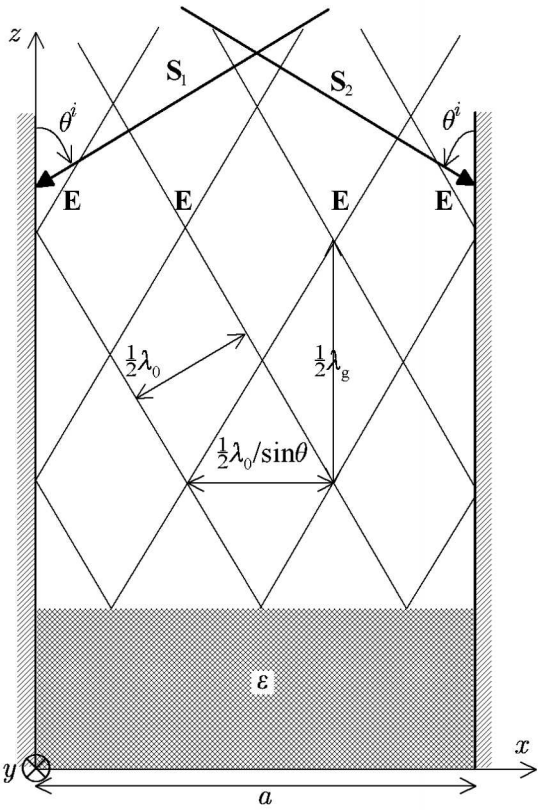

Figure 2.2. A metal trough with two TM-polarised rays.

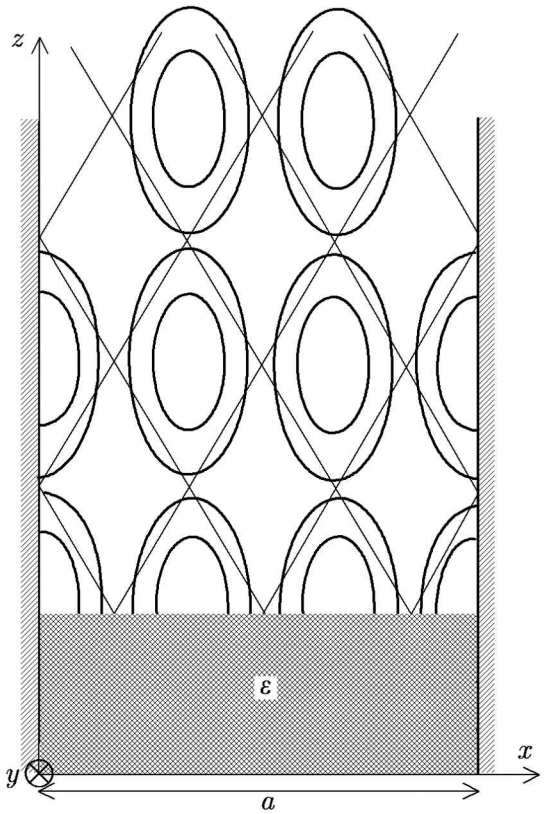

Figure 2.3. Vector E fields.

The simultaneous plane waves combine into a vector field, shown in figure 2.3. If there is a reflection at the dielectric boundary, there will be both a downwards and upwards propagating wave, creating a standing wave. The wave positions in figure 2.3 correspond to the standing wave pattern. The heating pattern of a single mode will be patchy, with heating minima where the vertical electric field dominates. This is discussed further in section 2.11.2.

The link between the horizontal indices (the number of standing halfwave variations) m and n of a cavity or waveguide having the corresponding dimensions a and b in the other directions x and y – and $\sin\theta^i$ is

$$\sin^2\theta^i = (\tfrac{1}{2}\lambda_0)^2 \cdot [(m/a)^2 + (n/b)^2] \qquad [2.5]$$

This equation has a limited number of integer solution pairs $(m; n)$ in each given interval of $\sin\theta^i$, as determined by the dimensions a, b, and the operating frequency interval. As a consequence, all possible combinations of $(m; n)$ for given values of a and b are represented by a finite set of $\sin\theta^i$ values.

The distance between the cold spots will theoretically be half a horizontal cavity mode pattern wavelength; this equals a/m or b/n and is thus always somewhat larger than the half wavelength in free space λ_0. However, the heating evenness can be improved either by the presence of several cavity modes, and/or rotation of the food load.

2.4 *Plane wave reflections at a flat surface*

When the direction of θ^i is at an angle, phenomena in accordance with Fresnel's laws in optics occur also

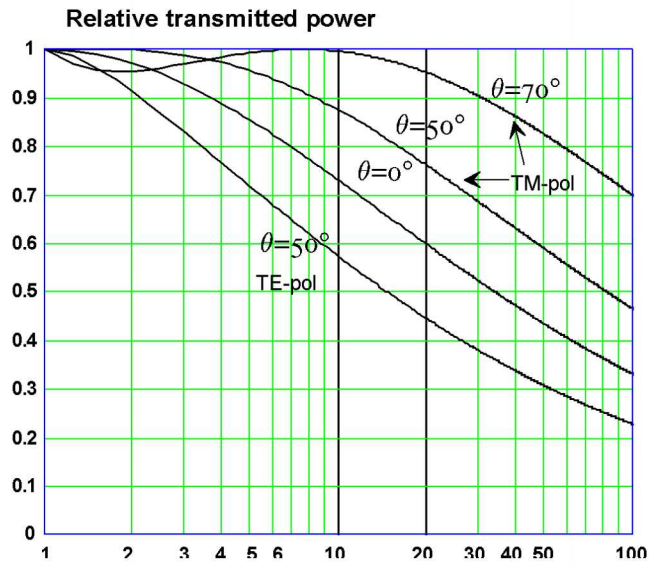

Figure 2.4. Power transmission into an infinitely thick dielectric with the incidence angle and polarisation as parameters.

with microwaves. With a dielectric load, TM-polarised incidence (TM modes) is of particular interest, since there is a condition of minimal reflection at the *Brewster angle* θ^i_B. It can be shown that

$$\theta^i_B \approx \arctan\sqrt{|\varepsilon|} \quad \sin^2\theta^i \approx \frac{|\varepsilon|}{|\varepsilon+1|} \qquad [2.6]$$

where index B is for this pseudo-Brewster condition for lossy dielectrics. It is of importance in microwave cavity studies and design that the mode wavelength λ_g in the z direction of *Brewster modes* can become much larger than the free space wavelength λ_0. The following applies:

$$\lambda_{B,g}/\lambda_0 \approx \sqrt{|\varepsilon_B|+1} \qquad [2.7]$$

The quotient $\lambda_{B,g}/\lambda_0$ becomes quite high for ε values typical of many load substances with a high water content, an example being $\lambda_{B,g}/\lambda_0=6$ for $|\varepsilon_B|=35$. The $\sin\theta^i$ interval of interest is thus rather narrow and close to the "cut-off" limit $\sin\theta^i=1$ which corresponds to striking incidence angle $\theta^i=90°$ and $\lambda_g\to\infty$.

It can be shown that the pseudo-Brewster mode reflection at the surface remains almost insignificant also for quite large $\varepsilon''/\varepsilon'$ values.

Fresnel's laws can be used to obtain the results shown in Figure 2.4:

- The reflected power remains low for all ε' values for foods if θ^i is 70° or more, with TM-polarised incidence.
- Perpendicular ($\theta^i=0$; TEM) irradiation gives a high reflection for high ε' values.
- TE-polarised irradiation is still worse than TEM incidence

Microwave oven cavity modes corresponding to TM-polarised incidence are thus more favourable. Microwaves are then absorbed with fewer reflections, which results in the performance becoming less sensitive to load item geometry and location variations. There are other advantages as well, which are discussed in the next section.

2.5 *Internal vertical standing waves in large flat loads*

It is often stated in the microwave oven literature that an important reason for uneven heating of food items is "internal total reflection". But Brewster-type modes are not reflected much at all at flat horizontal interfaces, neither when entering the top surface nor when leaving the bottom surface of the load item. Neither are any waves totally internally reflected. The waves leaving the bottom surface do not disappear but are instead reflected by the cavity bottom. When they

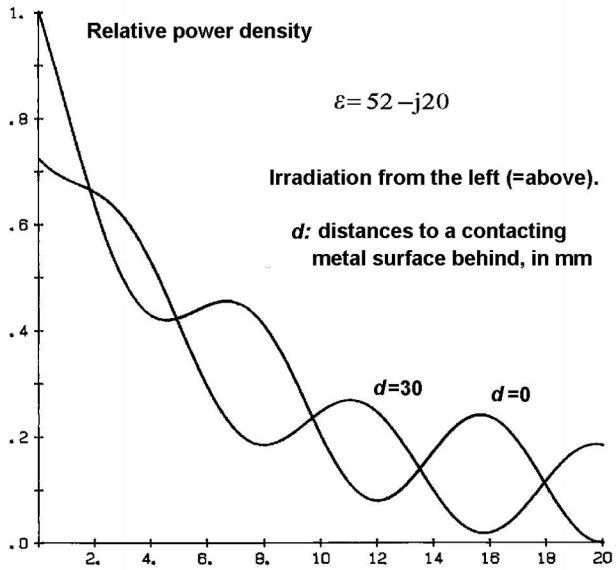

Figure 2.5. Theoretical power density pattern in a 20 mm thick slab under perpendicular plane wave incidence

return back through the load, a simple standing wave pattern is created. A second basic influence by ε' is then manifested: the waves inside the dielectric are slowed down by a factor $\sqrt{\varepsilon'}$, resulting in the wavelength in the direction of propagation being reduced by the same factor.

Figure 2.5 shows the solution obtained by calculations using the standard analytical so-called transverse resonance matrix method, for a 20 mm thick unidirectionally irradiated slab above a metal plane. The d_p of the material is 7,1 mm for all θ^i. – Two items are seen: there is a tendency for a maximum of the standing wave at the surface facing the incoming irradiation, and the location of the heating minima depend on the distance to the cavity metal bottom. The first item is due to the so-called magnetic wall effect, but occurs only if the retro-reflected wave escapes into free space. However, efficient microwave heating requires also the cavity ceiling to reflect microwaves back downwards, creating vertical standing waves. This also applies for Brewster modes, since the load does not cover the whole cavity bottom area. – The second item is that the escaping energy from the slab has to return, according to the energy principle.

Figure 2.6 shows what happens under realistic microwave oven conditions: the standing waves become much stronger, with almost no heating at all in the lowest minimum. The load is the same, and with horizontal dimensions 140 × 140 mm but now in the small

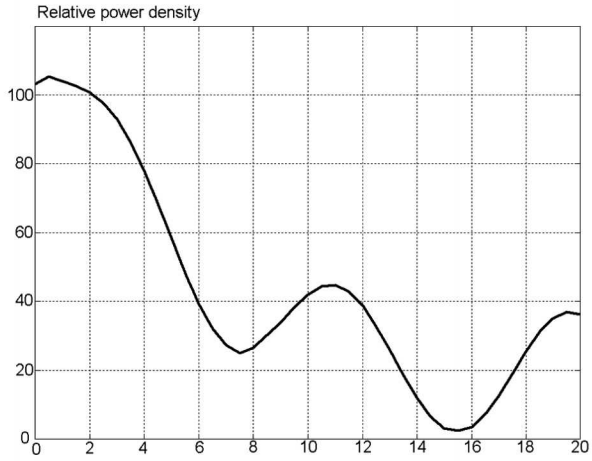

Figure 2.6. The numerically modelled vertical heating pattern in the centre of a 140×140 × 20 mm load with ε =52–j20, in the microwave oven in figure 2.9.

microwave oven of figure 2.9. The Quickwave™ software (QWED, 1997–) was used, with a resolution (cell height) of 0,5 mm. The power density in the vertical direction at the load centre is shown. The differences to the simpler analytical scenario result are mainly due to a realistic cavity mode pattern with retroreflected waves back down to the top of the load.

Actually, patterns like that in Figure 2.6 occur in most well-performing microwave ovens. The distance between maxima in the figure is about 8 mm, which corresponds well to $\frac{1}{2}\lambda_0/|\sqrt{\varepsilon'}| \approx 8{,}2$ mm.

The standing wave has stronger maxima and practically zero power density in the lowest minimum. This may result in unfavourable phenomena, such as power loss by stronger and earlier evaporation from the top surface, and a need for overall power reduction for allowing sufficient temperature evening-out by heat conduction. It is recommended to always assume a very uneven microwave heating pattern in the vertical direction in slab-shaped loads, with half an internal wavelength between the maxima.

One might think that internal total reflection would be significant if the food slab does not have parallel surfaces. This is not correct in practise, for two reasons: the cavity modes in "good" microwave ovens are typically TM-polarised, which reduces food surface reflections in general, and coupling phenomena of the trapped surface wave type at/under the load are different from those in geometric optics.

2.6 *Under-heating modes*

There is a shelf in all microwave ovens. Apart from the practical need for a flat surface to support the load, and the cleaning aspects, there is also a need to provide possibilities for the microwaves to reach the whole bottom surface of the load and thus also give heating from below – *under-heating*. The shelf is commonly of a microwave-transparent material such as borosilicate glass. Creation of sufficient under-heating is one of the essential targets in microwave oven development and does by no means occur by itself. Strong under-heating can actually be obtained in the bottom centre of slab-shaped loads having a diameter in excess of 20 cm, and there are actually some microwave oven models which typically provide about half the heating power from below for such loads on a recessed shelf. However, microwave oven performance test reports in consumer magazines also indirectly indicate that the under-heating is insufficient for such and similar loads in many other models. The performance of seemingly similar microwave ovens may thus vary considerably.

The geometry of the space below the load does not allow normal cavity volume modes, since the vertical height of the region below the food is less than half the free space wavelength. The particular trapped mode between the underside of the load and the cavity bottom is typically stabilised by the thick glass shelf and is characterised by having no vertical magnetic field. It is called a *longitudinal section magnetic (LSM) mode*. Such modes were first investigated and reported by Pincherle (1944). Their fields have pattern similarities to Brewster and other TM-type cavity modes with very long vertical wavelength, and can therefore be excited by such modes. Additionally, the

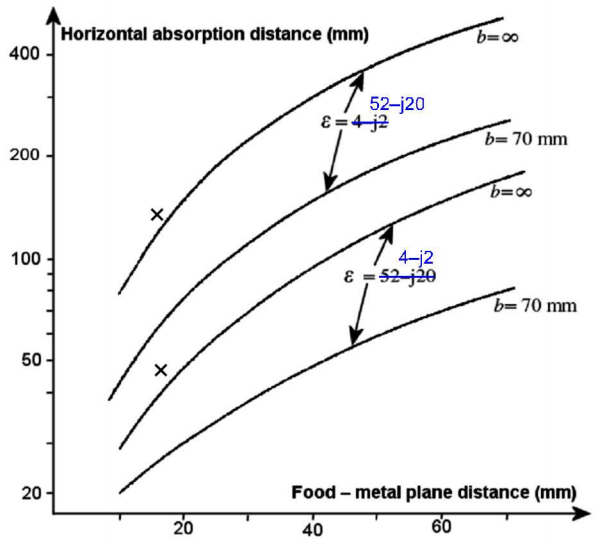

Figure 2.7. Trapped surface wave properties, 2450 MHz (from Risman, 1994)

favourable Brewster modes are typically of the so-called hybrid type, lacking the horizontal electric field in one direction, which is then the cavity depth (y) dimension (see figure 2.9).

A description of these LSM modes and their properties is given by Risman (1994). Figure 2-7 is from that work, and shows the horizontal absorption distance (that over which $\frac{1}{e}$ of the energy density at the load periphery of a thick load has been absorbed by the load) as function of the distance between its underside and the cavity bottom (without a shelf), with the load permittivity and a characteristic length b as parameters, at 2450 MHz. The parameter b is half the horizontal standing wavelength in the y direction (see figure 2.9), and the LSM mode propagation is in the $\pm x$ directions. The coupling of the cavity volume mode to the LSM mode is favourable when b equals the whole cavity depth dimension, which requires the mode index n of also the cavity volume mode in that direction to be 1.

It is commonly stated in the microwave literature that defrosting is problematic because an already thawed part absorbs more microwaves than a still frozen part. This phenomenon is sometimes called a runaway effect, but it can actually be overcome with LSM modes. The two crosses in figure 2.7 are for 20 mm airspace between the load underside and the cavity bottom, and for b (the cavity depth; y direction) about 300 mm. It is seen that the absorption distance is three times longer (120 mm) for the defrosted load (ε = 52–j20) as for the same load but now frozen (40 mm, for ε = 4–j2). This can be used to accomplish stronger power absorption of the LSM mode in the frozen food item. Actually, full power defrosting is now recommended in the user manuals for some household microwave oven models in the market. The LSM mode properties are then employed. Packaged food items defrosted at full power may allow the self-regulating effect to work better than if evening-out by heat conduction is promoted, as is the case with slow defrosting.

It may sometimes be difficult to separate the actions of cavity volume modes and under-heating modes in heating experiments with typical food loads. There are two common methods for experimental investigations. The first is useful with geometries similar to ready meals, and employs the heating pattern in the "IEC batter load" (IEC, 2006), as evidenced by partial solidification by microwave heating and subsequent pouring-off of the remaining unsolidified batter. A typical action of underheating modes is then the occurence of solidified regions in central areas of the

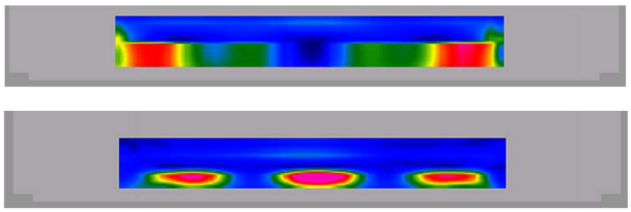

Figure 2.8. The under-heating power deposition pattern in the central long side vertical cross section of 160×110×20 mm loads with a horizontal thin metal sheet at half the height. Top image: ε =4–j1; bottom image: ε =52–j20.
See figure 2.23 for the colour scaling.

container bottom, with no corresponding solidified regions straight above. In contrast to this, cavity volume modes heating a raised batter load will give "hot spots" in the same inner horizontal positions in the top and bottom of the load, since the same modes are acting from both sides. – The second method employs a thin metal sheet at half the height of a load of for example mashed potatoes. A significant temperature rise in the lower part indicates the presence of under-heating modes. This is shown in the numerical modelling using the Quickwave™ software (QWED, 1997–) images in figure 2.8, with a scenario of a special microwave vending machine with microwave feed from above (Schönning and Risman, 2007) having a 20 mm high load separated into two by a thin horizontal metal plane at half height. The shorter horizontal absorption distance in the low-ε load is seen, and also that there is an LSM mode resonance with the high-ε load. It is also to be noted that volume mode heating of 10 mm high loads directly on a metal plane has a low efficiency (see chapter 18, section 18.3.1); this will increase when the metal sheet is removed.

Actually, the phenomenon just described is used with so-called crisp plates in some microwave oven models, for example by Whirlpool. Crisp plates are thin-wall aluminium frying pans with a thin ferrite rubber coating on the underside. This absorbs the magnetic fields of the LSM wave, so a combined frying (by the hot metal) and microwave cooking (by the volume modes from above) is obtained.

There has been, and still are, recommendations by some food manufacturers on raising food items to be defrosted in household microwave ovens. Either the outer packaging, or special so-called defrost racks, are then to be used as support. – As seen in Figure 2.7, any LSM mode action will now essentially vanish due to the too great absorption distance. But if there is no LSM wave excitation in the first place, cavity volume

modes may now persist around the whole raised food item, perhaps resulting in some heating of the underside also. Raising of the load may thus not improve the defrosting performance in ovens with significant LSM mode action. It may, however, help in ovens with weak or no LSM mode action.

It may finally be noted that the common statement in some microwave oven literature that a load height above the cavity floor of about $\frac{1}{4}\lambda_0$ provides "good impedance matching" is incorrect. The only situation where this may help some is for defrosting (see the example in figure 2.5, and with the oven in figure 2.9. which has essentially no LSM waves).

2.7 *Simultaneous heating of loads with different permittivities*

It is often stated in the literature that a frozen item next to a thawed item in a microwave oven is heated less. This is then explained by the larger penetration depth in the frozen item. However, this is not true with typical, reasonably well-performing microwave ovens. One must of course observe that the defrosting requires much energy and that the temperature changes slowly during the phase transition.

What actually happens can be explained by the behaviour of TM-type modes such as Brewster modes, as described in section 2.4. Additionally, the wave energy passing through the frozen load is reflected back into it, extending its "effective height". If they exist, the under-heating modes (see section 2.6) typically contribute by providing a stronger power absorption in lower permittivity loads.

Numerical modelling was used to obtain some illustrative results, using a representative microwave oven. A scenario with such a simple oven was presented by Risman (1998); data are given in Figure 2.9. The cavity is smaller than in typical ovens, but the scenario was carefully designed to represent several aspects of well-performing household microwave ovens. However, the under-heating mode is weak. There is a rotating turntable, so proper modelling for determinations of heating evenness has to be done with several positions of the turntable. Since the present objective is to describe heating mechanisms rather than to quantify overall performance, no rotation was used in the modelling described here.

The symmetry of the scenario allows direct comparisons of coupling efficiency and heating patterns of loads with different geometries and dielectric properties. A first layout is shown in figure 2.10, with the modelling results in figure 2.11. A vertical standing

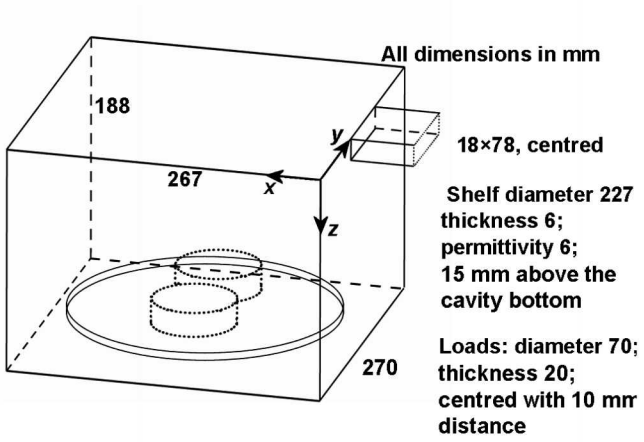

Figure 2.9. The small microwave oven scenario (Risman, 1998) with the two symmetrical loads.

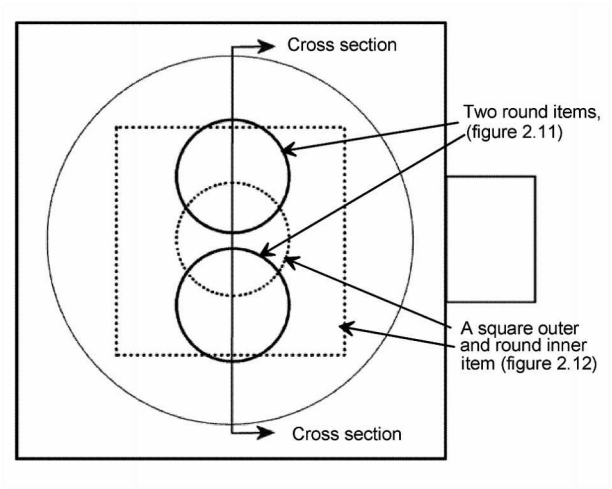

Figure 2.10. Top view of the small microwave oven, with the load configurations in figures 2.11 and 2.12

wave pattern is seen in the two loads with higher ε. A tendency of edge overheating (see section 2.9) is seen in the high-ε load but not in the others. The oven design, in combination with the low permittivity of the frozen load and its penetration depth being comparable to its height, results in a heating maximum in its bottom region. There is also heating from below in the load with intermediate permittivity. This result is due to the same type of standing wave phenomenon as shown in figure 2.6, and not any under-heating mode. Much the same is seen in Figure 2.12. The heating maximum in the bottom of the low permittivity part remains. It is caused by wave transmission through it, from above, and creation of a simple standing wave.

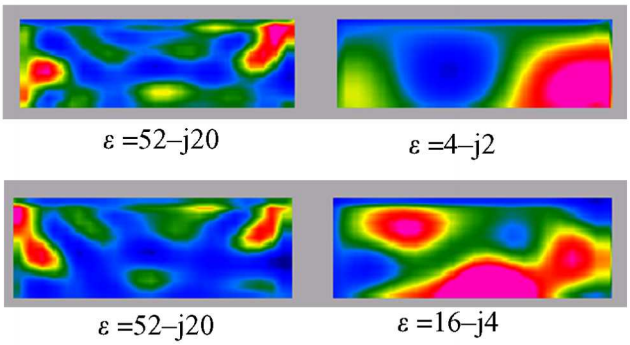

Figure 2.11. The modelled power density pattern in central vertical y-directed cross sections of two loads with diameter 70 mm height 20 mm, in the oven scenario in Figure 2.9 and 2.10.

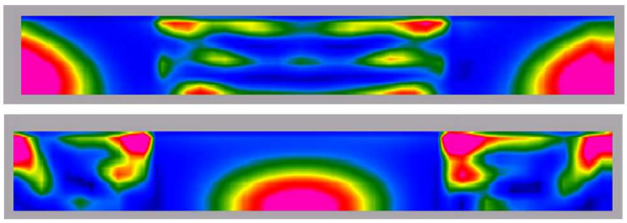

Figure 2.12. The modelled power density pattern in the central vertical y-directed cross sections of a square load with sides 140 mm and 20 mm height, with an included central circular load with diameter 70 mm; see figure 2.10. The square load in the top image has ε=4–j2 and the circular has ε=52–j20. The two permittivities are swapped in the bottom image.

2.8 Influences by different ε″, with the same ε′

As said in section 2.4, the wave reflection and thus the relative total absorption of the impinging power flux density, does not change much with the loss factor ε″. However, d_p changes. This is illustrated in figure 2.13, which also shows a consequence of the equal total power absorption in the two cases: the power density in the surface region becomes proportional to ε″. Of course, this applies fully only under the idealised conditions of the definition of d_p. However, it should be noted that it is normally unfavourable to have for example a salty sauce layer on a piece of meat: the sauce will be overheated, and also to some extent shield the underlying meat so that it gets less microwave power flux than if the sauce was less salty.

A food item such as cooked ham with a high salt content (see chapter 1, figure 1.5) has an increasing ε″ with temperature. This will result in an already hotter part to receive more microwave power. This dynamic

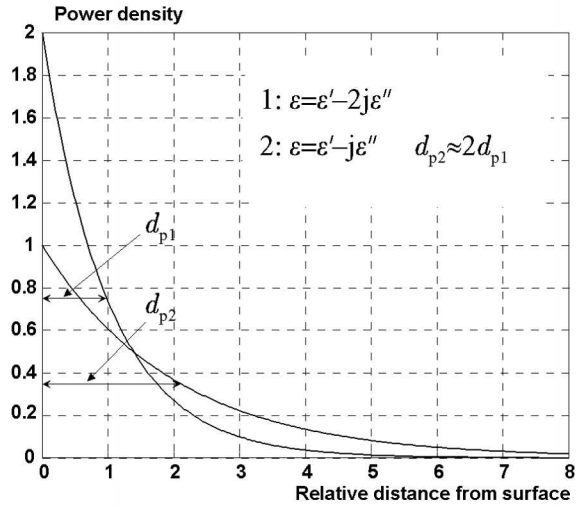

Figure 2.13. Comparative theoretical power dissipation in two large thick loads in the same heating cavity, with only different ε″

phenomenon is a well-known *runaway effect*. There are, however at least another, completely different, runaway effect (see section 2.11.7) , so this one can be called the *ε″ increase runaway effect.*

2.9 The edge overheating effect

This phenomenon is in many practical cases the most problematic kind of uneven heating. It has been, and is still, one of the major problems in achieving even heating of food items in microwave ovens as well as in industrial processes. It is a non-resonant diffraction phenomenon caused by the electric field component parallel to the edge of the item. This is TM-polarised incidence with the wedge axis now as reference, and is called TM_z here, to avoid confusion. High permittivity items create a more significant issue. However, the effect disappears for TE_z-polarised incidence, which corresponds to TM-type cavity volume modes (for horizontal edges). If these have a very long vertical wavelength, the edge overheating effect is also reduced on all horizontal edges, due to a vertical electric field then being dominant. This makes it possible to largely avoid edge overheating by particular designs of microwave ovens and industrial systems. It is indeed remarkable that this important phenomenon in microwave heating has not received the attention by academia it deserves, in comparison with cavity mode theory. A possible reason may be that analytical methods alone cannot be used to derive descriptive equations.

The effect is caused by diffraction which has to be non-resonant due to the fact that a wedge has no

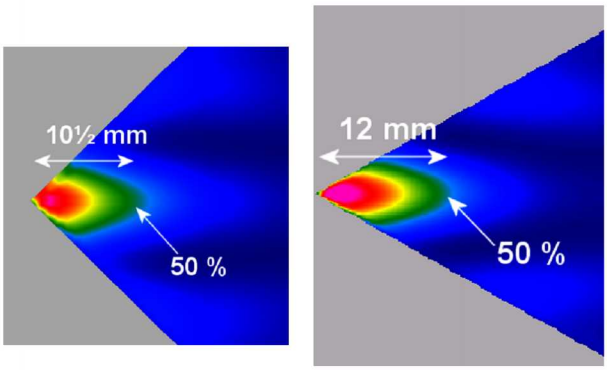

Figure 2.14 Relative power densities at 2450 MHz in a 90° (left) and 60° (right) wedge, ε=52–j20. Results obtained by free space modelling, with the electric field parallel to the edge and impinging from the left.

dimensional scale, as opposed to other simple geometries such as spheres and circular cylinders. The phenomenon is concentrated to a quite small region; see figure 2.14.

The strength of the phenomenon can be deduced by a first order theory, which has also been confirmed by numerical modelling and experiments (Risman, 2008). It turns out that the statements in many textbooks that the effect results from simple addition of wave energy irradiating the edge from two directions (from the side and from above, instead of one direction) is in error: for $\varepsilon' > 40$ and wedge angle 90°, the maximum power density in the tip is typically 4 times higher than some distance away from the tip, and 6 times higher for wedge angle 60°. For ε' about 15 the factor is about 2 for wedge angles between 30° and 60°. The effect has almost disappeared for $\varepsilon' = 4$. The size of the overheated zone also varies with ε'; the length 12 mm for the 60° wedge in figure 2.14 becomes 34 mm for $\varepsilon = 16 - j4$.

The first order equation for the electric field maximum E_ε inside the edge tip is

$$\frac{E_\varepsilon}{E^i} = \frac{2}{1+\sqrt{|\varepsilon|}} + \frac{0,50\cdot(90-\alpha)}{90+0,50\cdot\arcsin(1/\sqrt{|\varepsilon|})} \qquad [2.8]$$

where E^i is the incident field and the wedge angle is 2α. The first term is a wave potential term which also gives the field just inside a large flat load, and the second term a diffraction source term. The factor 0,50 is a so-called canonical constant that cannot be derived theoretically, and has been determined by numerical modelling (Risman, 2008).

It should finally be noted that the direction of incidence has a very small and only second order influence on the effect, as long as it is within the "free" (180–2α) angle. Impinging waves which do not hit the edge tip first will also create surface waves. The wave potential term will then change, and with that the edge overheating effect.

There is some additional information on edge overheating in section 2.11.3.

2.10 Heating of isolated rounded objects

2.10.1 Introduction

It is often said that microwaves heat "from the inside out". As has been shown earlier, that is generally not true, since the penetration depth d_p is shorter than the typical thickness of the food load. However, particular phenomena may be caused by the curvature of the load and by its overall size in relation to the free space wavelength of the microwaves. Its permittivity is of course also a basic variable, by determining the characteristic dimensions and strength of internal standing wave phenomena.

The first investigation of spheres and circular food cylinders by analytic calculations and experiments in 2450 MHz microwave ovens was made by Ohlsson and Risman (1978). They showed that very significant heating maxima occur in the centre regions of spherical objects with diameters from 20 to 75 mm, and circularly cylindrical objects with about 20 to 60 mm. However, no qualitative explanations were given.

The centre heating which may occur is often explained in the literature to be a result of quasi-optical refraction and internal total reflection, as would be the case for high permittivity ε' (the square root of which is the index of refraction) if the wavelength were much shorter than the curvature of the object. It is, however, obvious that the strength of the actual phenomena, as well as the small size of the hot spot in spherical objects, are such that that explanation is not correct. Instead, the effects are caused by *diffraction and resonant phenomena*, when the external fields vary so quickly in time that their free space wavelength λ_0 becomes comparable to the dimensions of the sphere. The resonant phenomena are of two basic kinds: internal and external (Gastine *et al*, 1967). Most of the diffraction field energy bound to the sphere is then inside and outside the object, respectively.

The theory for what happens when an electromagnetic plane wave hits a dielectric sphere that is small in relation to λ_0 was published very early (Mie, 1908). He studied scattering of light, which is that part of the diffraction which concerns the propagating modes or

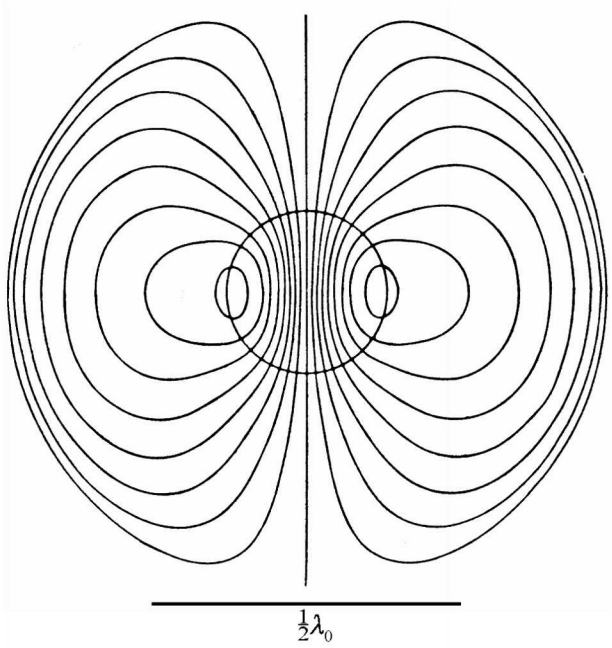

Figure 2.15. The magnetic field lines of the internal spherical TE_{101} resonance pattern of a free dielectric lossless sphere with ε =14 (from Gastine et al*, 1967). The first index (m) refers to the azimuthal variation, the second (n) to the equatorial and the third (p) to the radial.*

plane waves emanating from the scattering object. The scatterers were small lossless particles such as air molecules. He set up the equations in exact analytical functions, and showed that rather distinct internal resonance patterns may be set up. However, he could only make some very approximate manual calculations, since the complete trigonometric equation system is quite complicated. The first-order approximation for the scattering by very small bodies in relation to the wavelength λ_0 of light by air molecules had, however been earlier proven to be inversely proportional to λ_0^4 by Lord Rayleigh, thus explaining the blue sky.

For the calculations of the diffraction shown in the following figures, the complete analytical function solution procedures in the classical book by Stratton (1941) have been used. The Quickwave™ (1997–) software has been used for the numerical calculations.

2.10.2 Small spheres

In free space, the spherical TE_{101} mode (see figure 2.15, where indices are also defined) has the smallest radius at which an internal resonance occurs. The next internal resonant mode is TM_{101}, for a radius that is about 1,4 times larger than that for the TE_{101} mode. The TE_{101} mode pattern will thus be very dominant for

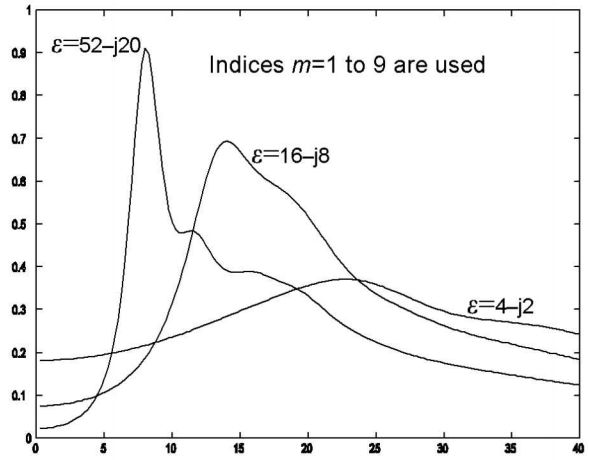

Figure 2.16. Relative absorbed power density ($1/r^3$; y axis) in free spheres under plane wave irradiation, as function of the radii in mm (x axis) and with ε as parameter, at 2450 MHz. Analytical calculations.

small spheres. Its resulting electric field, and by that the heating pattern, has the shape of a torus, Figure 2.15 shows the magnetic field and the associated electric field is maximal in the loop centre, i.e around the equator in the figure. Using the exact analytical solution, the resonant radius a_R for this mode becomes, for large ε′,

$$a_R \approx \frac{3,1 \cdot \lambda_0}{2\pi \cdot \sqrt{|\varepsilon|}} \quad (a_R \text{ in mm; } TE_{101} \text{ resonance}) \quad [2.9]$$

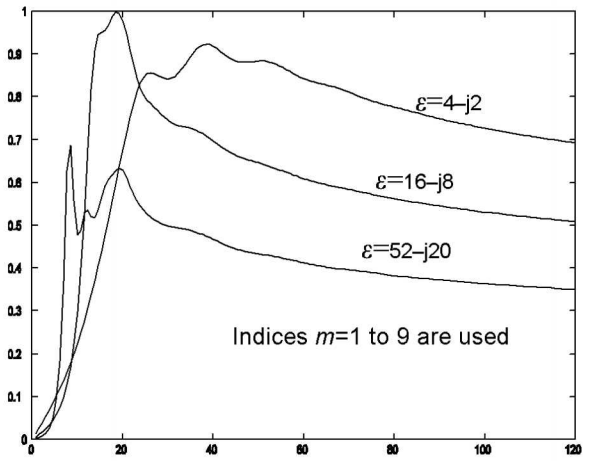

Figure 2.17. Relative absorbed power flux density ($1/r^2$, y axis) in free spheres under plane wave irradiation, as function of the radii in mm (x axis) and with ε as parameter, at 2450 MHz. Analytical calculations.

At 2450 MHz and for $\varepsilon' = 52$, this gives $a_R \approx$ 8,1 mm, i.e. a diameter of about 16 mm. For $\varepsilon' = 52/4=13$, the resonant radius doubles, to about 16 mm.

The next question is how significant the phenomenon may be. This can be assessed by figures 2.16 and 2.17, which illustrate the analytical equation calculation results for spheres with three different complex permittivities as function of their radii, at 2450 MHz.

It is seen in figure 2.16 that the relative averaged power density in the sphere is indeed quite sensitive to its radius for high-ε materials, with a dominating effect of the TE_{101} mode. However, the "antenna function" (i.e. the ability to efficiently absorb the impinging wave flux), illustrated in figure 2.17, is not so extreme. Additionally, another absorption mechanism

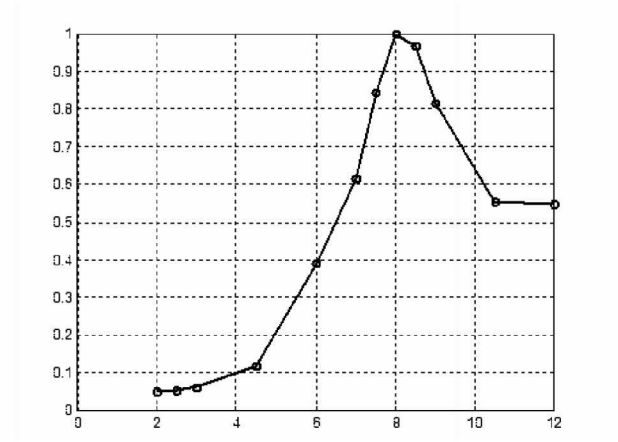

Figure 2.18. The averaged relative power density (y axis) in free spheres with ε =52–j20, under plane wave irradiation, as function of their radii (in mm, x axis). Computed numerically.

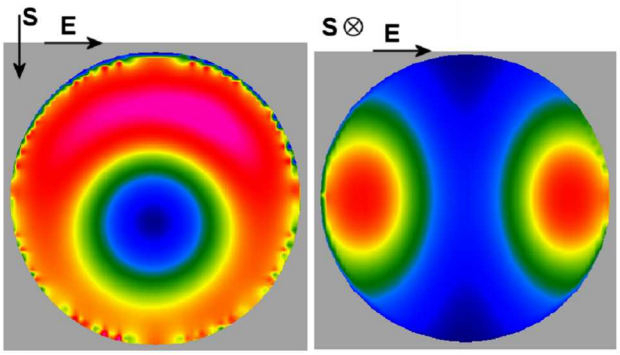

*Figure 2.19. The 2450 MHz power density pattern in an isolated 7½ mm radius, ε=52–j20, sphere irradiated by plane (TEM) wave. The **S** vector of irradiation direction is indicated, as is the wave polarisation (E = electric field). Computed numerically.*

that is obviously not an internal resonance effect is also seen in that figure. It is dealt with in section 2.10.3.

The maximum relative heating intensity for different diameters as determined by numerical modelling for spheres with ε=52–j20, is given in figure 2.18. When the radius reaches about 10 mm, the TE_{101} heating pattern begins to be taken over by that of the TM_{101} mode; the heating pattern maxima as seen in the right image in figure 2.19 then move towards the axis.

The first interesting phenomenon in addition to the resonance effect is the drastic reduction in power density when the diameter of the sphere is reduced. The slope is maximal between 6 and 7½ mm radius, but almost as steep up to the resonant radius which is about 8,1 mm in this case, according to equation 2.9. The absorption becomes proportional to r^6 in the steepest interval, which is even more than the Rayleigh scattering which is proportional to λ_0^{-4} for small scatterers. The power density reduction with size is thus so strong that there will be a significant heating unevenness when several small, separated and only slightly differently sized objects such as carrot dices are heated simultaneously.

The second interesting phenomenon is that the power density in successively smaller spheres approaches a constant value, as seen in figures 2.16 and 2.18. This occurs for radii smaller than about $\frac{1}{3}$ of the resonant one, i.e. about $2\frac{1}{2}$ mm for ε = 52–j20. Figure 2.16 indicates how small this quasistatic power density is in relation to that at TE_{101} resonance; it is a function of both ε' and ε'', since the so-called quality factor (Q value, resonance strength) depends on both. The electric field in the small sphere becomes constant and the ε' dependence, if ε'' is not large, follows the classical equation for the induced electrostatic field in a dielectric sphere:

$$dP/dV \propto \varepsilon'' \cdot [3/(\varepsilon' +2)]^2 \quad \text{(small sphere)} \qquad [2.10]$$

2.10.3 The exploding egg effect

This well-known phenomenon is manifested for example by a chicken egg in its basic shape, raw or boiled and deshelled, shattering violently in any microwave oven within about half a minute.

There are many explanations offered in the literature, such as a successive pressure build-up inside the shell, together with some kind of quasi-optical focusing of microwaves to its centre. These are wrong. Instead, an external diffraction resonance phenomenon occurs, resulting in a quite small but intense hot spot at the centre. In the case of the chicken egg, it seems as the

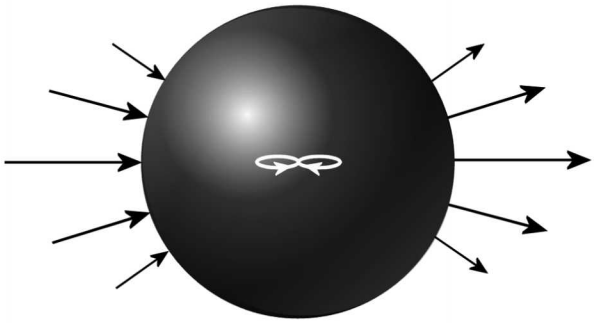

Figure 2.20. A schematic illustration of the instantaneous external resonant electric field pattern, and the internal power-generating magnetic field at the centre of a spherical load item, with the exploding egg phenomenon.

proteins inhibit normal boiling at temperatures above 100 °C, so a sudden release of steam occurs when the inhibition is no longer capable of withstanding the formation of a microscopic steam bubble. The pressure of the generated longitudinal sound wave then causes an avalanche effect of vapour bubble formation, within less than a millisecond. The hot spot temperature may exceed 135 °C at the time of shattering (Rothla and Risman, 1994).

Since most of the wave energy causing the hot spot is in this case on the outside and bound to the surface, the phenomenon as such is rather insensitive to the dielectric properties of the round object. Instead, its diameter, or rather circumference, must be in a certain interval for the phenomenon to become strong.

Actually, this can be seen in figure 2.17: there is a maximum of the absorbed power flux density for about 20 mm radius for ε=52–j20 as well as 16–j8. As said before, this cannot be traced in figure 2.16. This is consistent with the fact that only a small volume in relation to the whole is heated strongly.

It is also seen in figure 2.17 that there is a weak tendency at about twice the radius (40 mm) for all loads. That these radii correspond to about one and two wavelengths in circumference is not coincidental. Actually, the external field pattern is that of a standing so-called Zennek wave (Risman, 1994), which has a number of radially directed electric field maxima: two as seen in the explanatory figure 2.20 and then obviously four for the 40 mm radius sphere. The field pattern illustrated schematically in figure 2.20 is of the spherical TM_1 mode type (only an azimuthal variation; see figure 2.15 for co-ordinate definitions).

The chain of events begins with conditions for creating a standing TM_1 surface wave at the object. Since the pattern then becomes externally resonant and by that in time phase, the resulting pattern inside the object will propagate inwards with the same time phase everywhere, and thus set up a series of concentric ring-shaped standing waves. At the centre, a characteristic magnetic field pattern is then created, amplified by the converging wave energy. This induces strong currents which cause heating just at the centre.

It may again be noted that the phenomenon is not at all related to some geometric optics focusing effect. It

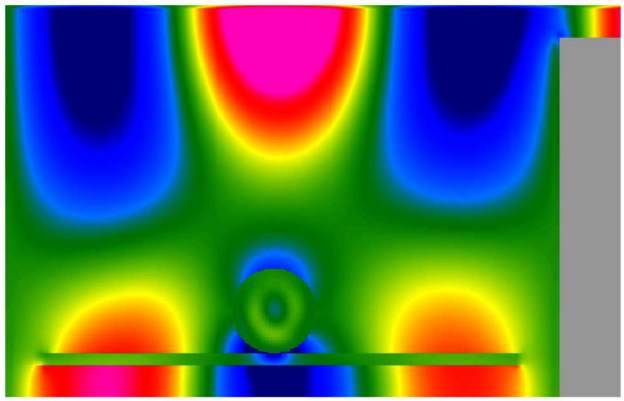

Figure 2.21. The instantaneous vertically directed electric field in the central vertical cross section of the model microwave oven in figure 2.9, with a 20 mm radius load with ε =52–j20. Magenta is maximum upwards-directed field and dark blue is maximum downwards-directed.

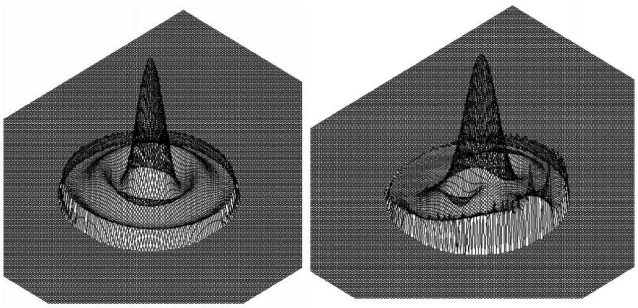

Figure 2.22. The power density pattern of the load in figure 2.21, in the same plane (right) and in the equatorial plane (left). – The radius of the volume in which the power density is larger than half the maximal is about 3,2 mm, corresponding to about 4 % of the overall volume. The average power density in most of the load volume is about 7 % of that at the centre.

is not difficult to calculate that such a focusing effect, with the wavelength being much shorter than the diameter, cannot result in the strong and concentrated centre heating that actually occurs.

An illustration of the effect – again using the microwave oven model in figure 2.9 – is shown in figure 2.21. It shows the instantaneous vertically directed electric field in the vertical central constant y plane, with a 40 mm diameter load with ε =52–j20 (corresponding to d_p = 7,1 mm). The field at the sphere has the same direction at the opposite top and bottom sides and is thus of the spherical TM_1 type. It is seen that the required fields of the surface wave resonance are in this case directly related to the cavity mode pattern, which is obviously of the TM type with index 3 in the plane of the figure. As also shown in figure 2.20, there is no need for the excitation fields to completely surround the spherical object.

The heating pattern in the same load plane as in figure 2.21 is shown in the right image of figure 2.22 (underside to the right). The left image (in the equatorial plane) clearly shows the ring-shaped standing wave pattern inside the sphere.

As a matter of fact, the same phenomenon occurs also in ellipsoidal and long circularly cylindrical objects, such as potatoes, small cups of coffee, etc. However, in such objects, the strong central overheating pattern becomes elongated. The hot zone may also be somewhat displaced from the axis.

Another consequence of the limited requirements on the external fields is that the phenomenon is not very sensitive to the load dimensions. This was verified already by Ohlsson and Risman (1978) and can be verified more easily now by numerical modelling. The following is then found:

- For ε=30–j12 (d_p = 9,1 mm), the radius of the hot spot (as defined in the 2.22 figure text) is about 5 mm, for all sphere radii between about 12 and 27 mm, at 2450 MHz. For smaller radii, the TE_{101} resonant pattern successively becomes significant.
- For ε=16–j4 ($d_p \approx$ 20 mm), the radius of the hot spot is about 6,8 mm and the average power density in a 20 mm radius item is now about 15 % of that in the centre.
- At 27 mm radius at ε =52–j20, the intensity at the centre is about half of that for 20 mm radius. This reduction is due to a combination of less favourable item curvature and the penetration depth effect.
- The hot spot intensity is largest around 20 mm radius, for in principle all ε' values.

It may finally be noted that as the effect becomes reduced by increasing curvature radius and thus increasing radial distance to the centre, conditions for quite even heating throughout in food items such as baked potatoes occur. Were it not for the exploding egg effect, fast microwave baking of large potatoes would not work!

2.10.4 The cold rim effect

External surface wave interference patterns do of course also occur for other geometries than spheres. The example now to be dealt with, the common shape of a short circular cylinder ("puck"), can only be studied by experiments and numerical (non-analytical) modelling.

A qualitative and quantitative description of the diffraction phenomena is given by Risman (2007), for thin (3 to 10 mm) flat circular high-ε lossy objects with radii 3…50 mm, under 2450 MHz irradiation with different polarisations. It is found that a peripheral cold rim of variable width occurs, with an inner circular ring-shaped or single hot area. The resulting heating pattern changes somewhat for lower permittivities, the inner hot ring then being replaced by centre heating with a wider cold rim. A suitable term for the phenomenon is therefore *the cold rim effect.*

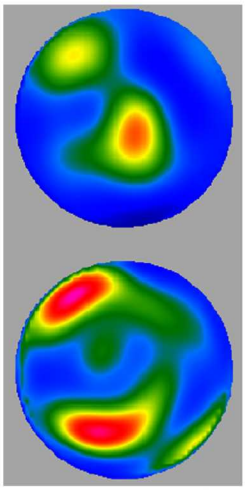

Figure 2.23a. The horizontal power density pattern in the top regions of two symmetrically located radius 35 mm, height 10 mm loads, in the oven of figure 2.9. The "upper" load has ε =16–j4 and the lower load ε = 52–j20.

Figure 2.23b (below). The power density pattern in the vertical cross sections of the loads in figure 2.23a. The left load has ε =52–j20; the right 16–j4. A standing wave pattern is seen in the left image.

Figure 2.23c (bottom) The colour scale in modelling.

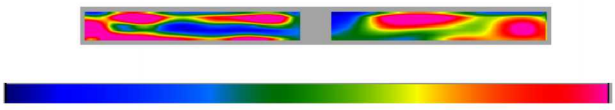

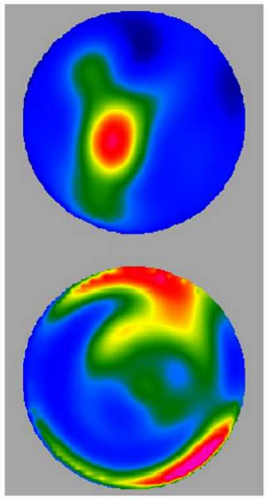

Figure 2.24. The horizontal power density pattern in the top region of two symmetrically located loads. All conditions and data are the same as those in figure 2.23, except that the loads are now 20 mm high.

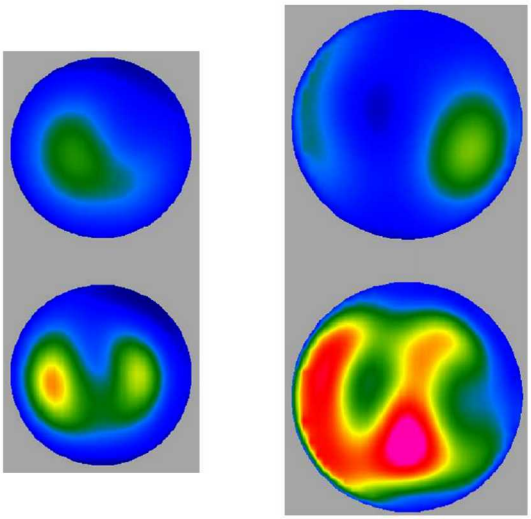

Figure 2.25. The cold rim effect for 20 and 25 mm radius loads, both with 10 mm height and in the oven of figure 2.9. The upper loads have ε=16–j4 and the lower ε=52–j20. The power density pattern is shown in the top region, and the amplitude scaling colour is the same for the two modelling runs.

Qualitatively, the cold rim is caused by two phenomena. The first occurs where the electric field component is parallel with the rim. The electric coupling slows down the propagation, resulting in creation of magnetic field components parallel to the axis, at essentially the same time phase (due to the high ε'), over the rim region. Since this is curved, a depletion of the coupled horizontal electric field occurs at the rim, as the induced currents will follow the shortest paths.

The second phenomenon occurs where the electric field is perpendicular to the rim. Due to the propagation slow-down, this external field will remain perpendicular around the rim surface in this region, and thus become weakened by approximately a factor ε' inside the object. The phenomenon is the same as with TE_z-polarised diffraction at a small dielectric cylinder. A very weak heating at the rim will result.

For small puck-shaped objects with medium high ε', the cold rim effect can also be explained by the creation of a field pattern similar to that of the spherical TM_{101} mode. The field pattern is then similar to that of the TE_{101} mode shown in figure 2.15, but with the electric and magnetic fields interchanged; it must also be noted that the radially directed electric field is discontinuous at the surface. Such an external field is actually similar to that of the spherical TM_1 mode shown in figure 2.20, indicating the generality of that type of diffraction effect.

Examples of the cold rim effect are shown in figures 2.23. The maximum heating area in the 11 o'clock direction of the high-ε load is not edge overheating, since there is a small cold rim at the periphery. Actually, there is no overheating anywhere at the periphery. The top region heating patterns in two similar loads is shown in figure 2.24, the only difference to the loads in figure 2.23 being that the load height is now 20 mm. In the high-permittivity load (lower image) there is now a hot ring almost all around, inside a narrow cold ring zone. In the low permittivity load, the hot zone is patchy and closer to the centre.

The cold rim effect may be quite sensitive to the load diameter. An example of this is shown in figure 2.25, which is the same scenario as in the previous figures, but now with load radii 25 mm and 20 mm, and 10 mm heights. The cold rims are wider in the radius 20 mm loads, and the microwaves couple less efficiently to them.

The cold rim effect may be significant for radii from 50 mm to 12 mm or less, for thin loads; up to more than 20 mm thickness for the larger radii and less than about half of the radius when this is small.

2.11 Combination effects

We have already seen the combination of underheating and cavity volume modes – which can of course be very advantageous. Some of the described effects can be said to have electric fields as their primary source, but others are instead primarily caused by the magnetic field. How do these act on the different microwave coupling phenomena to the load, and influence the power deposition patterns? Some basic considerations are given in section 2.11.1, followed by descriptions of some such combination effects.

2.11.1 *Some remarks on power absorption mechanisms*

The common equation given in the literature for the time average of the power density dP/dV in a lossy dielectric is

$$dP/dV = \pi f \varepsilon_0 \varepsilon'' |E|^2 \quad [2.11]$$

where ε_0 is the electric constant, f the frequency and E the internal electric field strength in the volume unit. The problem with this equation is that it may be very difficult to relate the internal field strength to the measurable field external to the load. It can therefore not be used in practical situations.

The basic expression for the power density is

$$dP/dV = -\tfrac{1}{2}\mathrm{Re}[\nabla\cdot(\mathbf{E}\times\mathbf{H}^*)] \quad [2.12]$$

where $\mathbf{H}$ is the vectorial magnetic field, ∇ the del operator and × the vectorial cross product. This indicates that both E and H are needed for power to be expended. This is in analogy to direct current power formulas: The power is $U{\cdot}I$ (voltage times current), but can also be expressed as $R{\cdot}I^2$ or U^2/R, where R is the resistance.

Which of the E and H fields dominate in determining the heating pattern? This basic question has different answers under different conditions. A hint is given by the boundary conditions at interfaces between different dielectric media: the H field is continuous, but the perpendicular E field component is reduced by a factor ε. Additionally, the fact that the parallel E field component is continuous across the interface is typically accompanied by a standing wave minimum of this external electric field at the surface of a high permittivity load.

2.11.2 *Horizontal heating patterns by cavity volume modes in large flats loads*

Since ε' is quite high, up to 70, for water and non-frozen non-dry food substances at 2450 MHz, the pattern of the magnetic (H) field will determine the heating pattern of such large flat load surfaces by cavity volume modes. The vertically directed electric (E) field will be substantially weakened just inside the load, and there is an H field minimum of the standing wave pattern of the cavity mode where this E field is maximum. *There will thus be a cold spot at the position of maximum vertical external E field.*

The same reasoning is applicable to susceptors, which are thin metal films, characterised by a film resistance in ohms per square. They will not be heated at all by a perpendicular electric field but instead by the parallel component (or, equivalently, by the parallel magnetic field inducing a current). Therefore, using susceptor films or fax papers for "cavity field mapping" as described in some literature, will not work unless used in different positions and sheet directions for confirming what are the mode types, including their polarisations and vertical wavelengths.

Can there be any direct heating of low permittivity loads by the vertical E field ? Obviously, the induced current by the H field will be weakened for low ε'. It turns out that equal heating intensities by the E and H fields in the cavity TM mode case requires the equivalent of

$$\sin^2\theta^i = \varepsilon'/3$$

(equal heating by TM mode E and H fields) [2.13]

Actually, this condition will not provide an even overall heating; it will be even only along some linear paths. However, the direct heating by the perpendicular E field may be still stronger in thin low-ε loads, which may then typically be advantageous.

2.11.3 *The edge overheating effect*

As said in section 2.9, the edge overheating effect is caused by a direct action of an electric field parallel to the edge tip. If the cavity volume mode has a low vertical impedance, the dominating fields will be a strong vertical electric field and a strong magnetic field in at least one horizontal direction, since the energy of the electric fields have to be equal to that of the magnetic when there is wave propagation. As a consequence, the horizontal electric fields are weak, and one of them may even be zero if the cavity mode is of the so-called rectangular hybrid type. The edge overheating effect will then become very weak.

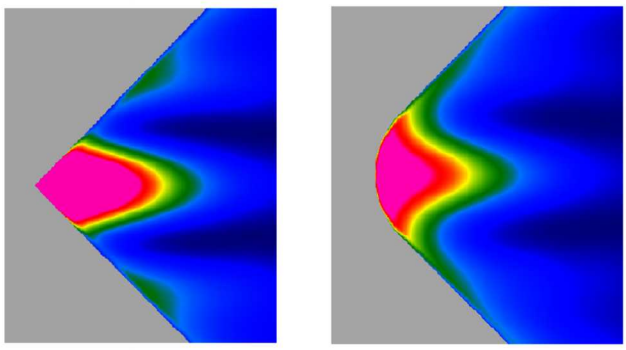

Figure 2.26. Edge overheating in a sharp and 12 mm radius edge. The intensity and geometric scales in the images are the same, but the amplitude at the tip is slightly more than twice as large in the sharp tip.

The heating intensity caused by a cavity volume mode in the main surface regions of large flat loads will be proportional to the loss factor ε''. This applies also to the edge overheating effect, so the runaway effect mentioned in section 2.8 may occur also here.

The power deposition in a rounded edge region will be different from the sharp edge case. The spreading-out of the heating pattern will, however, not be large. The reason is that another phenomenon will begin to play a role: the strong coupling of TM_z-polarised diffraction (the axis is reference) in a long isolated dielectric cylinder. Figure 2.26 shows two comparative heating patterns obtained by numerical modelling under conditions of free space irradiation.

2.11.4 Particular heating effects in uneven top surfaces

The small sphere TE_{101} diffraction resonance described in section 2.10.2 has two symmetry planes and can exist also in a small hemisphere. Small parts protruding over the mean surface may thus considerably modify the microwave coupling. This explains why it is typically difficult to obtain reproducible laboratory microwave heating results with heating of a semisolid food item such as mashed potatoes with a "rugged" top surface by imperfect spreading. It is better to use a smooth poured viscous surface such as the IEC batter (IEC, 2006).

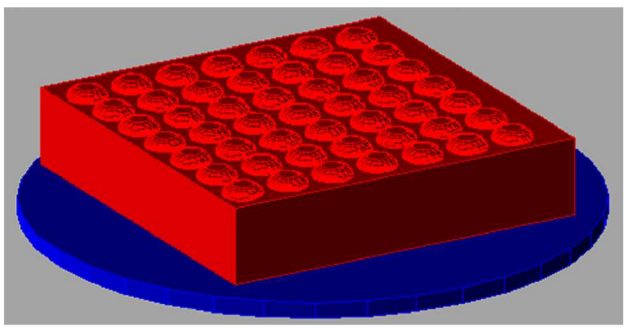

Figure 2.27. Example of a rugged top surface of a ready meal model. The rounded items are spherical segments with about 16 mm width and 3 mm height, on a 30×150×150 mm solid load.

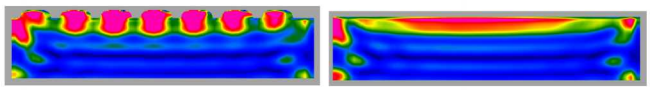

Figure 2.28. The power density pattern in the central cross section of the load in figure 2.27 and in a load with a flat top as comparison, in the vertical plane shown in figure 2.10 of the small microwave oven.

Figure 2.29. A commercially available microwave oven egg cooker. The spherical segment-shaped "holes" are 78 mm in diameter and 30 mm high; a normal chicken egg fills up to about 23 mm.

The rugged surface effect can also be intentionally used, to improve the overall evenness of heating over the top surface in ready meals. The examples shown in figures 2.27 and 2.28 are with ε =52–j20 throughout, and provides very significant small hot spots in the small spherical segments, which will not occur without them. This results in an improved heating of the top surface, and also a deeper wave penetration downwards, by some millimetres.

2.11.5 Combination of the cold rim and exploding egg effects

As seen in for example figure 2.23, there is a "hot ring" inside the edge of a puck-shaped load, and there is strong centre heating in a spherical object, as seen in for example figure 2.22. An example of a favourable combination effect of the two coupling mechanisms is offered by commercially available microwave egg cookers; see figure 2.29. Even if there are tendencies to centre overheating, this is sufficiently weak to allow quick denaturation without splutter. Even if the top edges have a small wedge angle, the cold rim effect for this curved top periphery essentially eliminates the edge overheating.

2.11.6 The hot corner effect

A rather typical heating pattern in a slab-shaped load in household microwave ovens – particularly models designed according to the so-called multimode principle with a ceiling stirrer or a rotating shelf – is shown

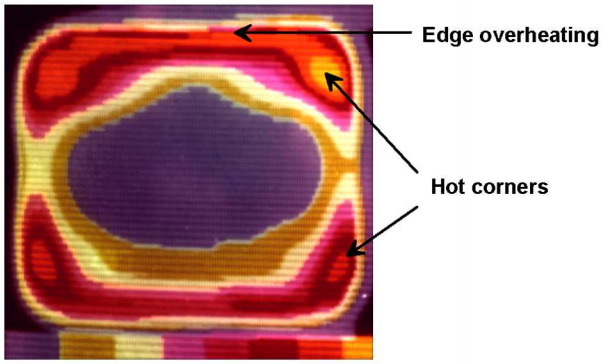

Figure 2.30. IR camera temperature pattern measurements on a 20×15 cm simulated flat food load in a multimode microwave oven with rotating shelf.

in figure 2.30. There is edge overheating and also hot corners, and a central cold region. Clearly, most of the unevenness pattern follows the rotating load rather than being controlled by cavity volume modes. The strength of the particular heating pattern, in relation to that primarily caused by the periodicity and combination of the cavity mode field patterns, does however vary between ovens. The reason for this variability is that the wave type builds up over a large part of the load surface, as opposed to for example the exploding egg effect.

The electromagnetic ray concept describes each cavity volume mode as a vectorial sum of typically four plane waves with the same angle of incidence and four symmetrical side angles. This may be used to explain the possibility of creation of surface waves of the Zennek type (Risman, 1994) propagating along the top surface of slab-shaped loads. They are characterised by the main electric field component being dominantly vertically directed out from the slab surface. The main feature of such waves is manifested when they encounter the "end" of the slab, where they are reflected back creating a standing wave. It is to be noted that this standing wave follows the slab end rather than the cavity volume mode pattern, and will therefore be maintained for rotating loads and for varying load surface sizes.

Figure 2.31 shows a plane wave free space scenario and figure 2.32 the numerical modelling result. Free space was chosen to obtain a better separation from other phenomena, and a TM-polarised impinging wave was used for obtaining reasonably good conditions for establishing a surface wave. It has most of its energy in the space above the slab and will encounter a region with higher impedance – the cavity space – at the slab "end" rim. This will result in a maximum of its standing electric field there, but this is

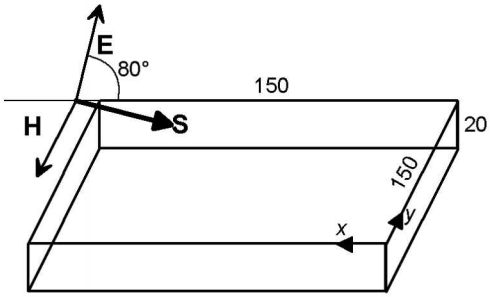

Figure 2.31. A plane wave free space modelling scenario. The load has ε = 52–j20.

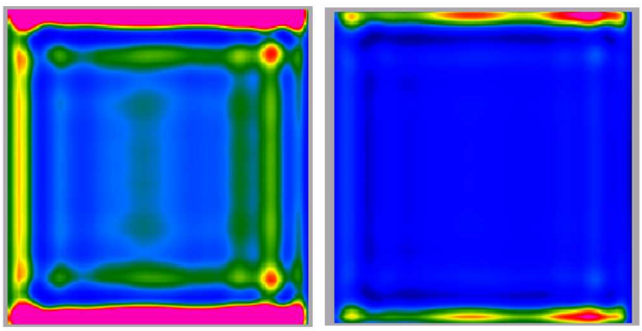

Figure 2.32. The power density pattern in the top region of the load in figure 2.31, obtained by numerical modelling. The wave impinges from the left. The amplitude scale level in the right image is set to a three times higher value for magenta .

essentially perpendicular to the slab surface and will thus not heat this rim much; see the left image in figure 2.29 at x =0. Since the electric field of the impinging wave is perpendicular to the left rim (x_{max}) this will not be heated much either. However, the horizontal component of the electric field will induce currents in the y =0 and y_{max} rims – the edge overheating effect. Surface waves propagating in the ±y directions will also be created at these rims.

The first interesting phenomenon is that the surface wave propagating in the –x direction will cause this edge overheating to be patchy, by a standing wave phenomenon as seen in the right image of figure 2.32. The maximum of this standing wave is always strongest some distance away from the "end" rim (x =0 in this case), and is thus primarily not determined by any cavity volume mode pattern.

The second interesting phenomenon is that the y-directed magnetic field vector accompanying the surface waves will become rotating at the rims and together with the impinging magnetic field induce maximum heating typically some distance inwards from the rims. This distance is in the order of 20 mm from the rims for high-ε loads and is strongest near

the x=0 rim in the figure, as a consequence of the chosen excitation. As is clearly seen in the left image in figure 2.32, these magnetic fields will interfere constructively at some distance 45° inwards from the corner. The corner edges will not be heated much, so there will be an often rather distinctive hot spot some distance inwards. This distance depends on the load permittivity and thickness – and of course also on the microwave frequency. For 20 and 30 mm rectangular thick loads with ε =52–j20 the distance the x and y directions is about 20 mm. It increases to about 26 mm for ε =32–j12.

The combination of the surface-wave induced standing edge-overheating wave near the corner tip and the constructive interference of the reflected magnetic fields from two adjacent straight rims causing an inner hot spot is *the hot corner effect*. It has to the knowledge of the author not been explained before, but attempts to tie the standing wave along the rim to cavity mode fields or even so-called circular wave functions has been published in some literature.

Interestingly, the strength of the hot corner effect increases some if the corner is rounded with radius 20 mm, but its position relative to the straight rims does not change. This effect is related to the exploding egg effect, by a radially directed electric field at the rounding.

How can the hot corner effect be minimised? – A first possibility is to avoid a flat top surface, but this must then be so uneven that there is an almost discontinuous edge. Another possibility is by rounding the corners of the food container, but the rounding must then be with a significantly larger radius than 20 mm. Replacing the single corner tip by two tips at some distance from each other (polygonal container shape) is another possibility. Paradoxically, a 20 mm radius may actually be worse than no rounding at all; the removed tip part would not be heated much at all by the microwaves. It would therefore improve temperature evening-out by heat conduction.

It should finally be pointed out that there is a relationship between the hot corner effect and the cold rim effect: if the rim is curved, the heating maximum will be some distance inwards from it. The necessary curvature requires the overall size of a load item subjected to the cold rim effect not to be large, whereas the hot corner effect can occur in larger load items. A general conclusion is therefore that food containers with large radii roundings are advantageous.

2.11.7 The burnt stripe effect

The cold rim effect (see section 2.10.4) is strong for thin semidry loads with radii less than about 35 mm (at 2450 MHz), which thus get a centre heating that cannot be modified much by the design of the microwave heating system. But a particular amplification of the heating in a typical narrow zone across the diameter in load items such as potato chips may also occur. An example is shown in figure 2.33.

If there would be only drying-out by the microwave energy, this would be faster in the central region. Since the permittivity then decreases and by that the absorption capability of these dryer parts, a negative feedback would then occur and even out the drying. But as is seen in figure 2.33 the burnt stripe effect is indeed a runaway phenomenon, where an already dried-out region absorbs additional power so burn marks are created. It is concluded that liquid water transport is necessary for the effect to occur.

What happens is illustrated in the numerical modelling scenario in figure 2.34. This shows a circular 24 mm diameter thin potato chip at 100 °C (permittivity ε = 50–j16), having an elliptical inclusion with axes 18 and 4 mm, representing a partially depleted region (permittivity ε =8–j1,6). It is irradiated from the left with a free space TM-polarised 2450 MHz wave with incidence angle θ^i = 82°; the magnetic source field is

Figure 2.33. A selection of four raw potato chips with diameter about 30 mm and thickness 4 mm, after partial drying in a microwave system providing dominant TM-polarised modes with no load movement. Note that the orientations are changed in the photo. – Courtesy of SIK, Sweden.

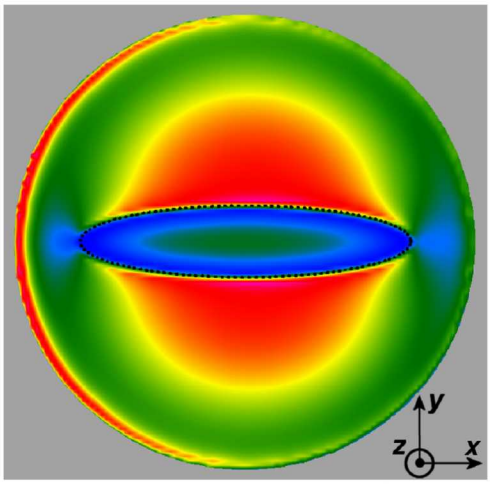

Figure 2.34. Modelling of a diameter 24 mm thin high-ε load with a central inclusion of a low-ε load, under TM-polarised incidence ($\theta^i = 82°$, from the left). (See text for further information.)

thus y-directed and the main current x-directed; the dominating electric field is z-directed.

The following phenomena can be distiguished:

- There is a heating (and thus current) concentration in the high-ε part close to the low-ε area. One can explain this as being due to the current following the shortest path and thus "avoiding" the low-ε area. The boundary is concave and not convex as is the case with the cold rim effect, so conditions are now reversed.
- There is a significant heating in the centre region of the low-ε area. This is due to direct action by the strong external z-directed electric field, as discussed in section 2.11.2. The phenomenon is amplified by the fact that the load is thin. It is to be noted that the heating intensity in the centre is almost half of the maximum in the non-depleted area, in spite of the ε'' being ten times lower and the penetration depth d_p being more than three times larger than in the non-dried region. This power density will indeed cause overheating, in consideration of the now limited amount of remaining water for evaporative cooling.
- There is a significant heating intensity minimum just inside the low-ε area boundary. This is a result of the z-directed electric field being almost short-circuited there, by the close high-ε area. One can also explain the minimum as a so-called magnetic wall effect. The minimum intensity is less than half of that in the centre of the low-ε area.

These sharp heating gradients result in the boundary between the outer relatively moist and the inner dry regions to become relatively constant, while the inner region continues to dry out. The resulting narrow burnt regions are clearly seen in figure 2.33.

Can this effect of uneven herting be avoided? Load rotation or TM-polarised field variations will not help much; the inner overheated region will then instead become symmetrically circular. The use of other microwave polarisations will result in edge overheating as well as a risk of lower microwave system efficiency. There are no easy solutions.

2.11.8 The multiple load item proximity effect

When experimenting with positioning of food items such as small potatoes, carrots, onions and meatballs in ready meal containers, it is not uncommon to experience so strong heating in the small contacting regions of such items that these may dry out or even burn. The causes of the phenomenon and some quantitative factors are now discussed.

A simplification is made by using spherical items with 16 mm diameter and exposing them to a plane wave. This will reduce the variabilities of phenomena caused by coincidental amplifications or weakenings by the overall positioning resulting from the variable cavity mode fields. The chosen diameter will provide a compromise between large and small surface areas being close.

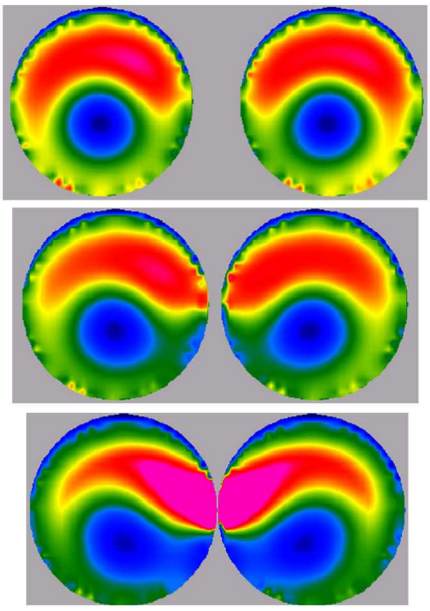

Figure 2.35. The numerically modelled power density pattern in the vertical central cross section of 16 mm diameter spheres with ε =52–j20, irradiated from above with the electric field in the plane of the paper, in free space.

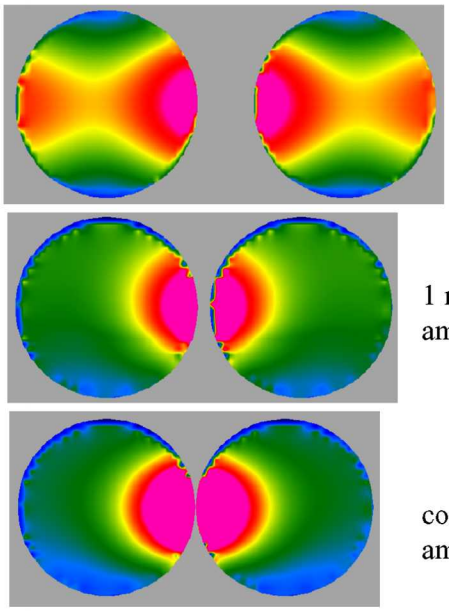

Figure 2.36. The numerically modelled power density pattern in the vertical central cross section of 16 mm diameter spheres with ε =16–j4, irradiated from above with the electric field in the plane of the paper, in free space. Amplitude values in the figure are for the magenta boundary; see figure 2.23 for the colour scaling.

Figure 2.35 shows three examples, with 4, 1 and 0 mm distance between spheres with ε =52–j20. The amplitude settings are at the magenta boundaries. In the 4 mm distance case, there is no coupling effect at all, and the maximum power density level can be set to 1. The maximum level goes up to 1,3 in the 1 mm case, and to 11 in the contacting case. There are thus two effects: a general increase of the power density with closer contact as stated in figure 2.35, and a drastic increase of the power density in the contacting spot.

The heating in the close contact area must be caused by a concentration of the displacement current, due to the requirement on its continuity in the region. The wave impedance of free space is about 377 Ω per square (see chapter 1.12.3) and is reduced by a factor $\sqrt{\varepsilon}$ in a dielectric. We now assume an effective capacitor surface area of the dielectric body of for example 4×4 mm, the current-carrying capacitance will become almost 8 times smaller in the airspace than in the bodies with ε = 52–j20. Thus, a distance in air of only ½ mm has the same capacitance as 4 mm inside the load. With the ½ mm airspace between the dielectric surfaces there will then very roughly be a comparable heating effect in the body in general and locally by the additional capacitive coupling.

If the permittivity of the spheres is instead 16–j4, the coupling phenomena would occur for larger distances between the items. Figure 2.36 shows the same three examples as in figure 2.35, but now with the spheres instead having ε =16–j4. There is now coupling also for 4 mm distance. It is about as strong as for the 1 mm distance in the ε=52–j20 case. The maximum power density level goes up to 1,4 for the 4 mm distance, to 3,7 in the 1 mm case and to about 20 in the contacting case. With permittivity 4–j2, the coupling becomes significant for slightly less than about 12 mm distance, i.e. 3 times larger than with ε = 16–j4.

The capacitance concept with unchanged capacitor area of the dielectric body would result in only about a doubling of the distance from the same effect. But a larger part of the lower-ε bodies participate in the effect as indicated by the size of the affected regions. One may therefore conclude that the effective coupling distances are approximately inversely proportional to the permittivity, at least for typical small objects of spherical shape.

As mentioned in the beginning of this section, the heating of small regions may become very strong. They will then dry out and by that reduce the capacitance and by that the effect – a negative feedback may occur. Even if burns or Maillard reaction discolouring may occur fires very rarely, if at all, start by the close contact effect. For that to happen, arcs between quite sharp edges or points of food substances containing parts with high fat or sugar content are needed; see chapter 1, section 1.9.3.

It is stated in some literature that this and other phenomena is caused by an internal total reflection effect related to the internal standing waves and resonant patterns dealt with in sections 2.5, 2.10.2 and 2.10.3. However, the wavelength of the microwaves is comparable to the characteristic sizes of food items and these are furthermore so curved that geometric optics concepts are not applicable anyway; the fields as such have instead to be studied, as is done here and in previous sections. The quasistatic capacitance concept provides sufficient coupling data for most practical purposes.

2.12 Summary and conclusions

The heating result – both the heating patterns and the microwave coupling efficiency – depend on a multitude of separable parameters. There are two such important parameters which depend on the design of the oven cavity or applicator and its feed structure: volume mode polarisations with their vertical wavelengths, and the presence and strength of under-

heating trapped surface wave modes. These mode types behave differently as functions of the load permittivity.

Twelve distinct phenomena which depend on the load permittivity and geometry have been described – see the list in section 2.1. Some of these are interrelated, and all are to a varying extent dependent on the load permittivity.

Modern, efficient software for numerical microwave modelling has been commercially available for about ten years and this chapter provides many illustrations of its use. Analytical calculations are possible for only some few simple load geometries, so modelling is an indispensable tool not only for simulating actual heating experiments but also towards qualitative understanding and practically oriented quantifications of the various phenomena described in this chapter. Separation of the phenomena additionally provides possibilities to construct new and efficient goal functions for automated optimisation computations.

Acknowledgement

Thanks to Per Floberg, formerly at SIK – the Swedish Institute for Food and Biotechnology, for valuable discussions and recommendations.

References

Gastine M *et al* (1967) '*Electromagnetic resonances of free dielectric spheres*' IEEE Trans. MTT-15(12), p694–700.

IEC (2006) *Household microwave ovens – methods for measuring performance. Consolidated edition 3.2*, IEC, Geneva.

Mie G (1908) Ann. Physik 25, p377. (Also in Stratton, 1941)

Ohlsson T and Risman P O (1978) '*Temperature distribution of microwave heating – spheres and cylinders*', J Microwave Power Vol 13(4) p303–309.

Pincherle, L (1944) '*Electromagnetic waves in metal tubes filled longitudinally with two dielectrics*', Physical Review, 66(5) p118–130.

QWED Sp. z o.o. (1997–) *QuickWave™ software for electromagnetic design*, www.qwed.eu.

Risman, P O (1991) '*Terminology and notation of microwave power and electromagnetic energy*'. J. Microwave Power & Electromagnetic Energy 26(4), 243–250.

Risman P O (1994) '*Confined modes between a lossy slab load and a metal plane as determined by a waveguide trough model*' J. Microwave Power & Electromagnetic Energy 29(3), 161–170.

Risman P O (1998) '*A microwave oven model – examples of microwave heating computations*' Microwave World (IMPI) 19(1) p20–23.

Risman, P O (2003) '*Understanding microwave heating in cavities in use today*', AMPERE conference, Loughborough UK.

Risman, P O (2007) '*Puddles and droplets – an investigation of their influences on microwave system performance*', IMPI symposium, Vancouver Canada.

Risman P O (2008) '*Diffraction phenomena inside dielectric wedges – qualitative theory and verification by modelling and experiment*', MIKON 2008 conference paper A7/1, Wroclaw, Poland.

Rothla M and Risman P O (1994) '*Splutter of foods during microwave heating*', IMPI symposium digest, p26–29.

Schönning U and Risman P O (2007) '*A microwave system for direct frozen-to-hot vending applications*' IMPI symposium, Boston USA.

Stratton, J A (1941) *Electromagnetic theory*, McGraw-Hill Book Co, London.

Sundberg M (1998) *Analysis of industrial microwave ovens*, PhD thesis No 332, Chalmers University of Technology, Göteborg Sweden.
